RSC Advances

ROYAL SOCIETY OF CHEMISTRY

www.rsc.org/advances

Table of contents entry

A Versatile Ambient Pressure Drying Approach to Synthesize Silica-based Composite Aerogels

Jin Wang, Yong Wei, Weina He and Xuetong Zhang*

A general ambient pressure drying approach to synthesize silica-based compositre aerogels with high BET surfaces and large pore volumes has been reported.

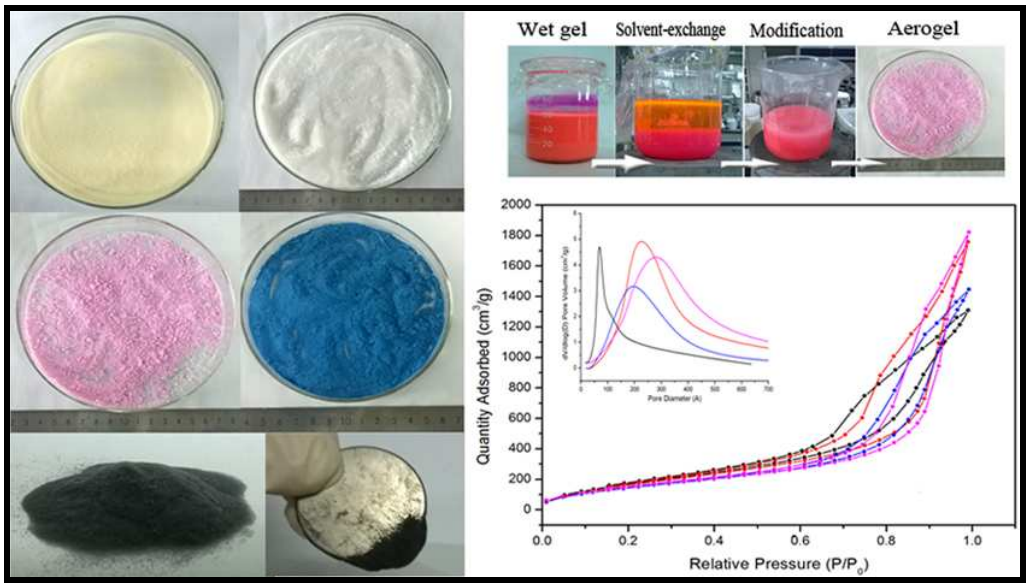

A Versatile Ambient Pressure Drying Approach to Synthesize Silica-based Composite Aerogels

Jin Wang[1] Yong Wei[1] Weina He[1] and Xuetong Zhang[*1,2]

[1]Suzhou Institute of Nao-Tech and Nano-Bionics, Chinese Academy of Sciences, Suzhou, 215123, P. R. China. [2]School of Materials Science and Engineering, Beijing Institute of Technology, Beijing, 100081, P. R. China.

* Corresponding author: zhangxtchina@yahoo.com

Abstract: A versatile ambient pressure drying (APD) method for synthesizing silica aerogels as well as silica-based composite aerogels with different colors or functions has been developed in this work. Presented polyethoxydisiloxane (PEDS) under base condition in ethanol, alcogels were obtained; followed by hexane solvent-exchange and pore surface modification, the wet-gels were dried under ambient pressure at temperatures ranging from 25 to 150 ^{o}C to produce silica aerogels with high BET surface areas and low thermal conductivities. Introduced various guests, e.g., dyes, Fe_3O_4 nanoparticles and Ag nano-wires in the sol-gel process, colored, magnetic or bio-functional silica aerogels were synthesized by the APD method. All the products were of high BET surface areas varying from 500 to 1000 m^2/g and of average pore sizes in the range of 8-20 nm, regardless of the drying temperature and the presence of dye molecules or nano-particles embedded. The tapping densities of the aerogels were in the range of 0.03 to 0.2 g/cm^3, and the thermal conductivities were found varying from 0.022 to 0.040 W/mK. Moreover, the structures and morphologies of the aerogels were investigated by FTIR and SEM, respectively. The stability of the colored aerogels was studied by UV-vis spectrometer, and the results indicated that the dyes were embedded in the aerogels and may be gradually released. Furthermore, the capacity of the magnetic aerogels for wastewater treatment was investigated. In general, an APD method involving a single hexane-exchange step has been developed, and various silica-based composite aerogels prepared by APD is achieved, which show a great potential to synthesize silica aerogel and its hybrid aerogel in the industrial scale.

1. Introduction

Microporous and mesoporous materials have attracted extensively interests from both academy and industry due to their significant structure properties such as high porosity and high specific surface areas, which are widely used as drug delivery systems[1], tissue scaffold[2], filtration[3], catalyst loading[4], energy storage[5], and thermal insulation[6], etc. Among them, aerogels are the most highly porous materials currently available, and have a high porosity (～98%), large surface area (up to 1200 m^2/g), low density (down to 0.003 g/cm^3), and extremely low thermal conductivity (～0.012W/mK)[7,8.] Though the silica aerogels were first discovered by Kistler[9,10] in the early 1930s, it's only recently that silica aerogels have attracting growing interests, especially in the aim of large scale manufacture of silica aerogels due to their advantages mentioned above and its widely application in thermal insulation[11-17].

Aerogels are normally synthesized by the supercritical extraction of the pore liquid from wet gels, which is expensive and is hard to fabricate large dimensional aerogels. Therefore, industrial-scale production of aerogels is restricted. In order to solve these problems, the ambient pressure drying (APD) method has been proposed via solvent-exchange with low surface tension solvents and surface modification of the wet gels[18], in which the silylated surfaces do not participate in condensation reactions or hydrogen bonding as the gel is collapsed by the capillary tension developed during drying. Therefore as the liquid-vapour recede into the gel interior, the shrunken elastic network progressively spring-back toward its original porous state. However, solvent-exchange is a lengthy and tedious process[19,20], which usually takes several days or weeks. Recently, economic and large-scale industrial production of silica aerogels by APD has been developed and the time of production is remarkably

reduced to one day[21,22]. Nevertheless, to our best knowledge, all the aerogels prepared by APD are involving large amount of water washing or proton exchange, ethanol wash or exchange, and finally hexane exchange and modification, which consume extensive solvents and the more solvent-exchange steps involved, the more possibility to result in environmental pollution. Thereafter, how to avoid water-washing and multi-steps of solvent-exchange in synthesis of aerogels, for instance, developing a method only involved hexane exchange and modification (no water wash and ethanol exchange), is an attracting topic, which may not only considerably reduce the fabrication time and imparts on environment, but also reduce the fabrication costs.

Meanwhile, composite and functional aerogels are another interesting topic. For example, the composition of silica and polymers can significantly improve the mechanical properties as compared to pure silica aerogels[23,24], and the composition of silica and TiO_2, B_4C can reduce the thermal conductivity of silica aerogels by the prevention of thermal radiation[25]. The composite aerogels, however, were normally prepared by supercritical liquid drying (SCD) method. The synthesis of silica-based composite aerogels and functional aerogels via APD method is rare, one example is the synthesize of titania-silica aerogel-like microspheres by a water-in-oil emulsion method reported by Gan et al.[26] In order to fulfill industrial scale production of composite aerogels, neither the SCD nor the present APD technology is desired because the SCD limits the large scale fabrication while the present APD involves water-wash and ethanol exchange, which may wash out the composite components especially when the hybrids are dyes.

In order to solve the problems mentioned above, we developed a simple APD method to

synthesize silica aerogels and its composite aerogels without any water-wash and ethanol solvent-exchange in the present work. As illustrated in Scheme 1, polyethoxydisiloxane (PEDS), which can be easily prepared from tetraethoxysilane (TEOS)[27-31], was used as the precursors for three reasons: (1) PEDS can be directly gelation in alcohol under base condition, therefore, the alcogels can directly solvent-exchange with hexane; (2) there where still plenty of ethoxy groups on the backbone, which can significantly reduced the amount of modification reagents (such as trimethylchlorosilane (TMCS) and hexamethyldisilazane (HMDS)); and (3) by introducing dyes and other components at the sol-gel process, composite silica aerogels can be produced by the APD in large scale.

Thus, silica aerogels were synthesized by using TMCS and HMDS as the modification reagents via the APD method proposed in Scheme 1. Moreover, the impacts of drying temperatures on the structure and physical properties of the aerogels were also investigated. Appling the same APD method, various silica-based organic and inorganic composite aerogels showing different colors or functions were synthesized. For example, methyl orange, rhodamine B, victoria blue B, $CuCl_2$, Fe_3O_4, and Ag nano-wires were successfully embedded in the silica aerogels. FTIR, thermal conductivity, BET measurements were conducted and the results indicate that the BET surface areas and thermal conductivity etc. of the composite aerogels were not significantly affected but even improved.

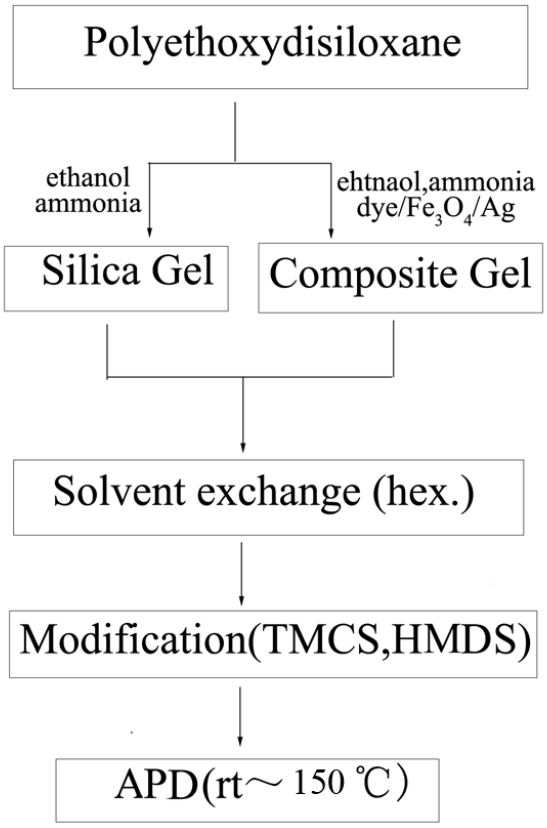

Scheme 1. A flow chart showing experimental procedures for the synthesis of silica aerogels and silica-based composite aerogels.

2. Experimental

2.1 Materials

TEOS, methyl orange, rhodamine B, victoria blue B (Aladdin Industrial Corporation), and TMCS, HMDS (TCI) are used as received. Nano Fe_3O_4 particles with average diameter of 20 nm were used (Aladdin Industrial Corporation). Ag nano-wires was prepared according to literature[32] and used as ethylene glycol solution stabilized by polyvinypyrrolidone (PVP). PEDS was prepared according to literature[28], the molar ratio of TEOS: water: ethanol is 1:1.3:2.5. Other reagents are of analytical pure and used as received.

2.2 Synthesis of silica aerogels by APD

Silica aerogels were prepared according to Scheme 1. By using the sample prepared shown in Table 1 entry 3 as example: PEDS (30g) were dissolved in 200 ml ethanol and stirred in a 500 ml flask for 10 min, then 500 μl ammonium hydroxide was added drop-by-drop into the PEDS solution and gelation was occurred in 30 min. After aging at 40 ^{o}C for 2 h, the alcogel was crushed and vigorous stirring in 200 ml hexane for 5 h. The gels were collected by filtration or centrifugation and again vigorous stirring in 200 ml hexane for another 5 h. Finally, the gels were modified by TMCS (5 ml) in 100 ml hexane for 2 h and dried after filtration at 150 ^{o}C for 30 min.

2.3 Synthesis of colored silica aerogels by APD

The colored composite silica aerogels were synthesized via the APD method, the same to that described above for the pure silica aerogels. The only difference is the addition of a small amount of dye or metal salt into the PEDS solution before gelation.

2.4 Synthesis of magnetic silica aerogels and Ag nano-wire-silica composite aerogels via APD

Functional silica aerogels were also synthesized via the APD method as described in section 2.2. Similar to the method of synthesize colorful aerogels, Fe_3O_4 nano-particles and Ag nano-wires were added in the sol-gel process. It should be noted that, for synthesizing Fe_3O_4-silica composite gels, more than 2 ml ammonium hydroxide must be added. The gelation occurred under stirring so that the Fe_3O_4 nano-particle can be uniformly dispersed in the silica networks. Moreover, HMDS should be used as modification reagent.

2.5 Characterization

The pore size distributions and average pore diameters of the aerogels were analyzed by the BJH nitrogen adsorption and desorption method (ASAP 2020, Micromeritics, USA). The

surface areas of the aerogels were determined by the Brunauer-Emmett-Teller (BET) method, based on the amount of N_2 adsorbed at pressures $0.05< P/P_0<0.3$. The cumulative pore volume was measured at the point $P/P_0 = 0.99$. The FTIR spectra were measured on Thermo Scientific Nicolet iN10 spectrometer using a transmission mode. The UV-vis spectra were determined on UV-1800, the scanning range is from 300 to 800 nm. The thermal conductivity of the aerogel powders under room temperature were measured by using transient hot wire method (XIATECH C2000, China), the data was collected for three times with 5 min interval of each measurement. The micro-structural studies of some selected aerogels were performed using field-emission scanning electron microscopy (Quanta 400 FEG). The samples were coated with Au nano-powder under current of 20 mA for 1 min. TEM measurement was carried on a Tecnai G2 F20 S-TWIN. Samples were prepared by dispersing aerogel powders in ethanol and dropped onto a copper grid, finally, it is dried under air for one week. The areogels densities were the tapping densities in this work.

3. Results and discussion

3.1 The synthesis of silica aerogels and their physical properties

The APD method to synthesize silica aerogels has been developed as contrary to supercritical liquid drying, where the supercritical conditions are not needed and the ambient pressure is enough thanks to the spring-back effects[18]. In order to scale-up the synthesis of aerogels for industrial production, sodium silicate has been widely used as precursors due to it's lower cost as compared to TEOS and trimethoxysilane (TMOS)[21,22]. However, tedious water-wash should be carried out when sodium silicate was used, and before solvent exchange with hexane, alcohol exchange for the water is required. Moreover, a large amount of

modification reagents such as TMCS are essential (side reactions between TMCS and alcohol and water are significant). These processes are increasing the fabrication costs and time, and the risk for pollution. In order to simplify the approach for large scale production of silica aerogels, PEDS was used as precursors because it's commercially available and can be easily prepared from TEOS. More importantly, as illustrated in Scheme 1, no water-wash and alcohol exchange was needed. The wet-gels can be directly underwent hexane exchange and modified with a very small amount of TMCS or HMDS because there are plenty of hydrophobic $–OCH_2CH_3$ on the Si backbone, rather than the –OH groups (This can be confirmed by FTIR spectrometer and will be discussed in the following section). By introducing dyes or other functional component in the sol-gel process, composite silica aerogels would be synthesized by this APD method.

To confirm this proposal, silica aerogels were prepared by a sol-gel process from PEDS, after aging for ca. 2 h, the gel was solvent-exchanged with hexane and modified with TMCS or HMDS. Finally, the modified gels were dried at room temperature or 150 ^{o}C under ambient pressure. As a control, xerogel was prepared via the same method without modification. The products are shown in Figure 1. Silica aerogels were successfully synthesized for the samples modified with a little amount of TMCS or HMDS (Figure 1c, d, e, and f), while stiff, glass-like xerogels were formed for the samples without modification (Figure 1a and b). Moreover, as can be seen in Figure 1, the aerogels dried at 150 ^{o}C forming liquid like powders, while that dried at room temperatures are small bricks but can be easily smashed into liquid like powders. Thus, silica aerogels are prepared by the simplified APD, even under ambient pressure and ambient temperatures.

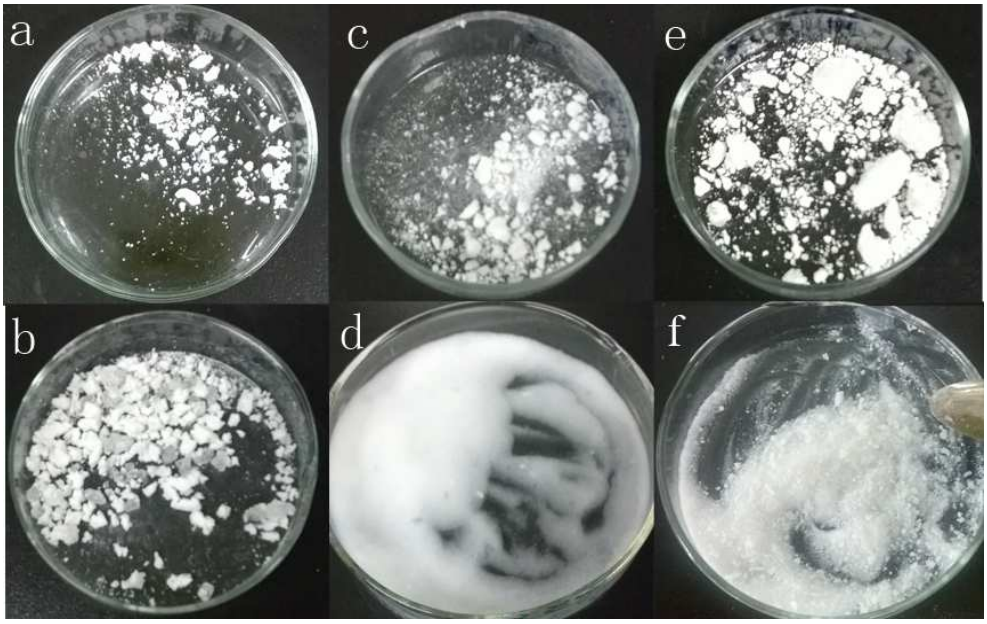

Figure 1. Photo images of aerogels made by APD at room temperature: (a) without modification, (c) modified with TMCS, (e) modified with HMDS; by APD at 150 ^{o}C: (b) without modification, (d) modified with TMCS, and (f) modified with HMDS.

In order to investigate the effects of drying temperature on the structure and physical properties of aerogels, three batches of aerogels were prepared from the same modified wet gels by drying at 25, 80 and 150 ^{o}C, respectively. Their tapping densities, BET surface areas, average pore diameters, pore volume and thermal conductivities were characterized and the results are presented in Table 1(entry 1- 3). The N_2 adsorption-desorption isotherms of the aerogels are shown in Figure 2, and the pore size distribution curves are given in Figure 3. As can been seen, the physisorption isotherms obtained for all the silica aerogels exhibit hysteresis loops, which are due to the characteristic features of mesoporous materials (Type IV isothems). From Table 1, we can conclude that the BET surface areas, average pore diameters and pore volume are all increased with the increased drying temperature, which may possibly due to a better spring-back effect under higher temperature[18]. High BET surface

areas of 925.01 m^2/g and very low thermal conductivity of 0.0237 W/mK was achieved when the silica aerogels dried at 150 ^oC. Interestingly, High BET surface areas of 880.23 m^2/g and very low thermal conductivity of 0.0240 W/mK was obtained even when the silica aerogel was dried at room temperature. The properties of silica aerogel modified by HMDS and dried at 150 ^oC are shown in Table 1. The low tapping density (34.1 mg/cm^3), high surface areas (835.52 m^2/g) and high pore volume (2.45 cm^3/g) indicated that the silica aerogels can also prepared by using HMDS as the modification reagent.

Table 1. Structure and physical parameters of the silica aerogels.

Entry[a]	Modification reagent[b]	Drying Temperature (^oC)	Density (mg/cm^3)	Surface areas (m^2/g)	Average pore diameter (nm)	Pore volume (cm^3/g)	Thermal conductivity (W/mK)
1	TMCS	25	69.0	880.23	9.4	2.18	0.0240
2	TMCS	80	36.7	905.81	11.6	2.50	0.0241
3	TMCS	150	58.5	925.01	13.5	2.73	0.0237
4	HMDS	150	34.1	835.52	10.1	2.45	0.0241

[a] 30g PEDS dissolved in 200ml ethanol as determined from the feed molar ratio of TEOS; [b] 5% (in volume) of TMCS or HMDS in hexane.

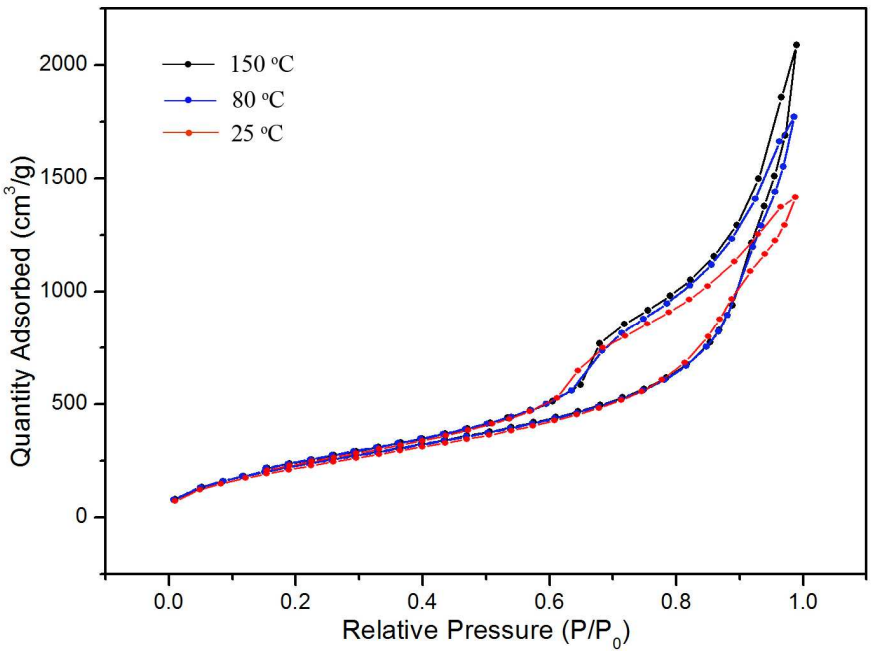

Figure 2. N_2 adsorption-desorption isotherms of silica aerogels via APD at indicated

temperatures (entry 1-3 presented in table 1).

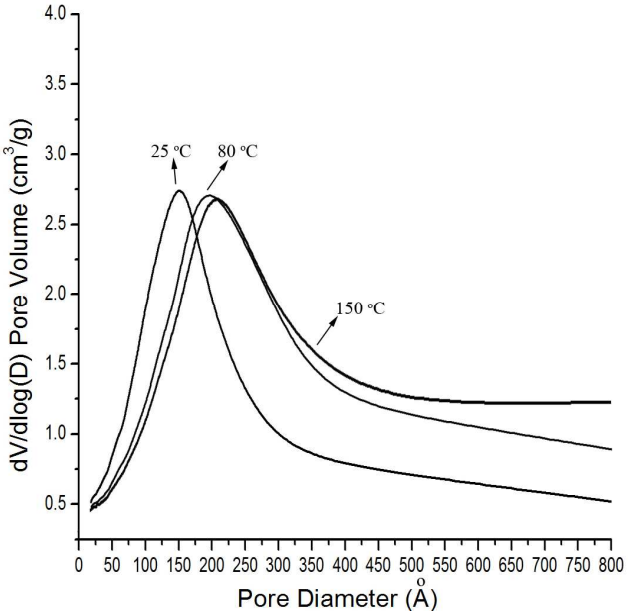

Figure 3. Pore size distributions of silica aerogels dried at indicated temperatures.

The chemical structures of the aerogels were confirmed by FTIR spectra as shown in Figure 4. Xerogel (Figure 1b) synthesized without modification (Figure 4a) exhibits a broad absorption park at 3450 cm^{-1}, corresponding to the vibrations of –OH. Moreover, the strong peaks locate at 2790 to 2980 cm^{-1} demonstrated that plenty of $–OCH_2CH_3$ groups are exist in the system. As a result, a relative small amount of modification reagents can be work well (5% in volume). Figure 4b and c shows the FTIR spectra of silica aerogels modified with TMCS (entry 3) and HMDS (entry 4), respectively. There are two peaks appearing at 840 and 1360 cm^{-1} as compared to Figure 4a, which are corresponding to the vibrations of Si-C. Besides, the –OH peak at 3450 cm^{-1} is almost unobservable in the silica aerogels. These results indicated that the –OH groups has been successfully replaced by $–Si(CH_3)_3$.

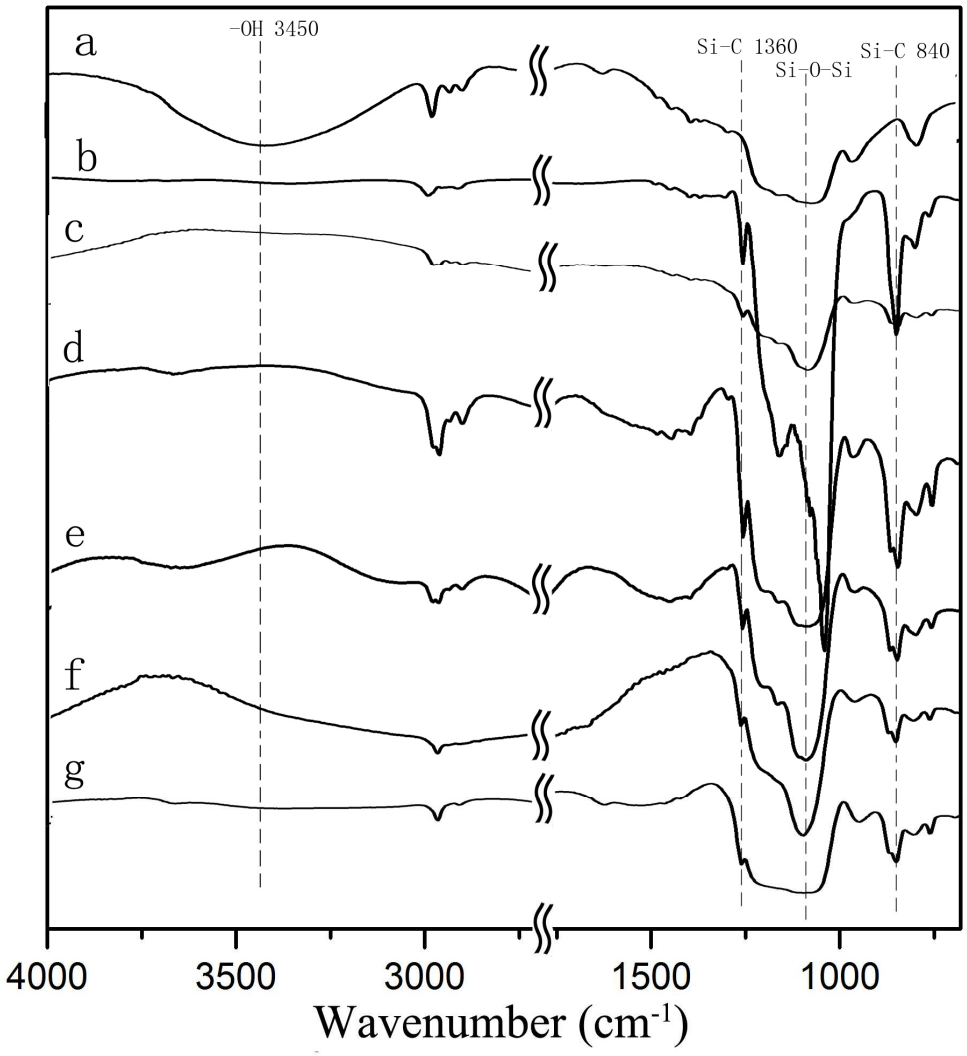

Figure 4. FTIR spectra of the aerogels: (a) silica xerogel without modification, (b) silica aerogel modified with TMCS (entry 3), (c) silica aerogel modified with HMDS (entry 4), (d) Rhodamine B-silica composite aerogel modified with TMCS (entry 7), (e) Victoria blue B-silica composite aerogel modified with TMCS (entry 8), (f) Ag nano-wire-silica composite aerogel modified with HMDS (entry 14), and (g) Fe_3O_4-silica composite aerogel modified with HMDS (entry10).

3.2 Colored silica aerogels and dye releasing behaviors

Because there is no water-wash and alcohol exchange in the simplified APD method,

colorful silica aerogels may be produced by the APD method based on the facts that dyes or metal ions can dissolved in ethanol but insoluble in hexane or cannot be completely wash out by hexane-exchange after embedded in the silica networks. Therefore, $CuCl_2$, methyl orange, rhodamine B, and victoria blue B were added in the sol-gel process to synthesize colored aerogels as shown in Scheme 1. The images of the colored silica aerogels are shown in Figure 5, and their structure and physical properties are summarized in Table 2. The $CuCl_2$, methyl orange, rhodamine B, and victoria blue B -silica composite aerogels are yellow, light pink, bright pink, and blue, respectively. Though 5 w/w% of the dyes are embedded in the aerogels, the taping density, BET surface areas, and thermal conductivity are not apparently affected. For instance, the thermal conductivities of colored aerogels are lower than 0.030 W/mK except for $CuCl_2$ composite aerogels, while the BET surface area of the methyl orange-silica composite areogels is 931.62 m^2/g. The pore diameters of the aerogels are smaller than 20 nm. When compared to the pore volumes of pure silica aerogels presented in Table 1, extremely high pore volume are obtained for the organic dye composite silica aerogels, from 3.05 to 3.53 cm^3/g of the victoria blue B-composite aerogels and the methyl orange-composite aerogels, respectively. The reason is not very clear at present, but from the pore distribution cures shown in Figure 3 and Figure 6, a broad pore distribution and large pore diameters were observed in the dye-composite aerogels, which may contribute to a relative larger pore volume.

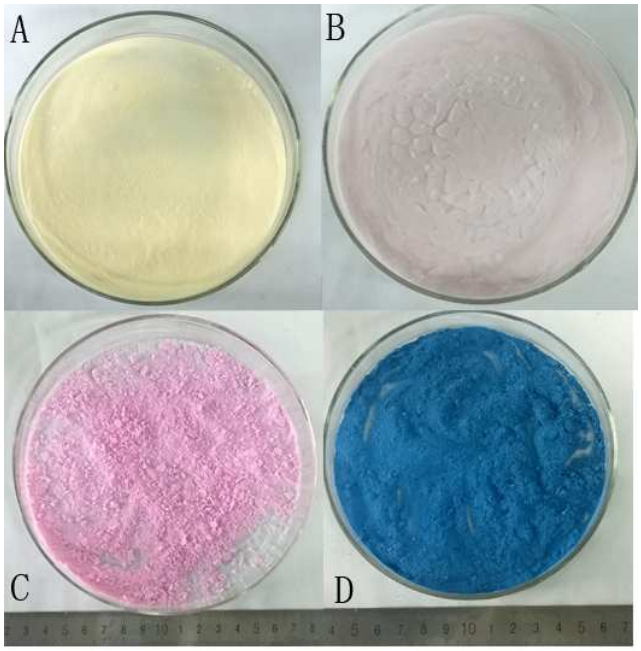

Figure 5. Photo images of colored aerogel powers: (A) $CuCl_2$-silica, (B) Methyl orange-silica, (C) Rhodamine B-silica, and (D) Victoria blue B-silica composite aerogels.

Table 2. Structure and physical parameters of the dye-silica composite aerogels.

Entry[a]	Dye/metallic oxide	Density (mg/cm^3)	Surface areas (m^2/g)	Average pore diameter (nm)	Pore volume (cm^3/g)	Thermal conductivity (W/mK)
5	$CuCl_2$	105.0	736.76	8.7	1.70	0.0356
6	Methyl orange	58.6	931.62	17.8	3.54	0.0221
7	Rhodamine B	58.1	850.35	11.2	3.05	0.0248
8	Victoria blue B	49.5	910.01	9.2	3.23	0.0298

[a] The drying temperature is 150°C, the modification reagent is TMCS, and the amount of dye to silica is 5 % by weight.

Figure 4 d and e shows the FTIR spectrum of the pink (entry 7) and blue (entry 8) aerogels, respectively. Similar to that of pure silica aerogels in entry 3 and 4, two peaks appearing at 840 and 1360 cm^{-1} that correspond to the vibrations of Si-C has been observed. Besides, the –OH peak at 3450 cm^{-1} is almost unobservable in the colored silica aerogels. These results indicate that the existence of dyes does not prohibit the modification process. The N_2 adsorption-desorption isotherms of the colored aerogels shown in Figure 6 exhibit similar type IV isothems with hysteresis loops to that of pure silica aerogels (entry 1-3), which

indicate that the dye molecules may not form large particles that blocking the mesoporous holes. The SEM image (Figure 7) shows the micro-morphology of the colored aerogels. Uniform nano-particle networks can be clearly seen from Figure 7A (blue aerogel), which is coincident with the narrow pore size distribution as shown in Figure 6 (insert figure, blue line). In the SEM images of the rhodamine B-silica composite aerogels (Figure 7B) and methyl orange-silica composite aerogels (Figure 7C), nano-particles can also been observed. However, the pores are not as uniformly as that victoria blue B-silica aerogels. The wider pore size distributions of two aerogels are obvious as shown in Figure 6 (insert figure, red and pink line).

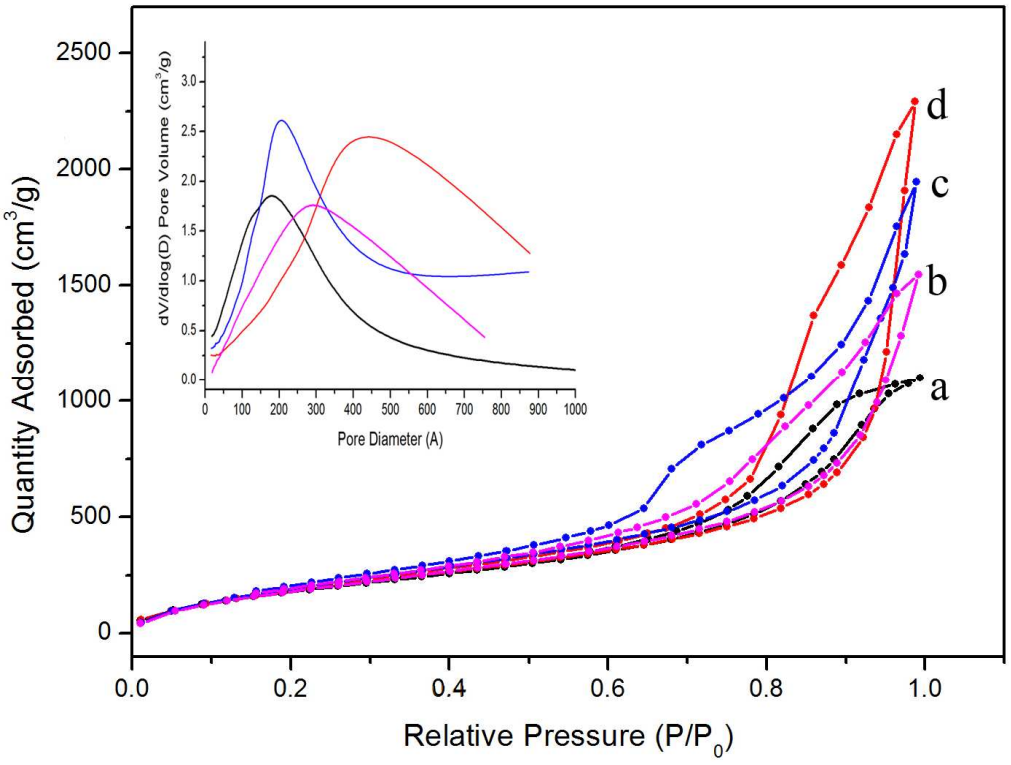

Figure 6. N_2 adsorption-desorption isotherms of colored silica aerogels: (a) entry 5, (b) entry 7, (c) entry 8, and (d) entry 6. The inserted figure is the pore size distributions of the corresponding aerogels.

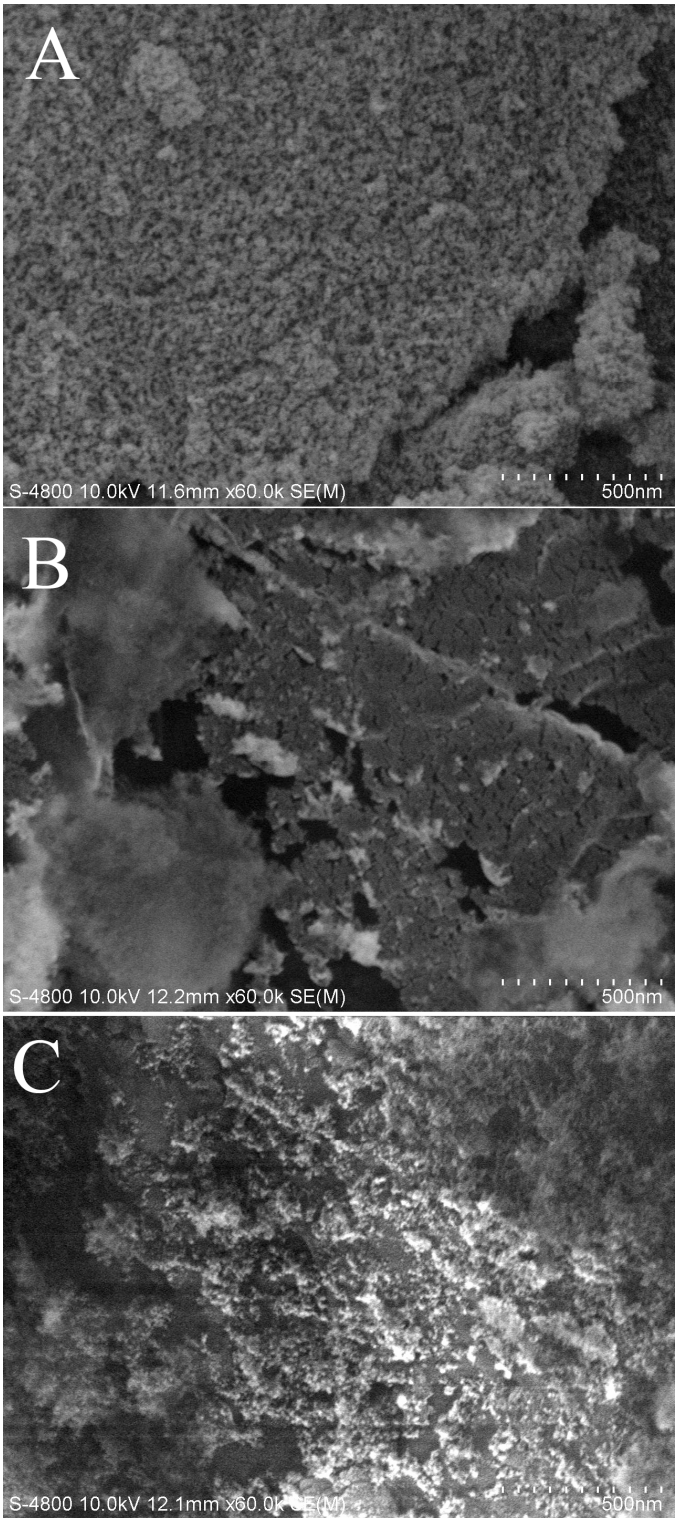

Figure 7. SEM images of: (A) Victoria blue B-silica composite aerogel, (B) Rhodamine B-silica composite aerogel, and (C) Methyl Orange-silica composite aerogel.

The stability of the colored aerogels was studied by UV-vis spectrometer by suspending the

colored aerogels in distilled water. As shown in the photos in Figure 8, the aerogels are hydrophobic and the dyes cannot be washed out even under vigorous stirring in the first few days. However, after continuous immersing in water for one month, victoria blue B and methyl orange were slightly released into the water, as can be seen in the photo on the top-right site of Figure 8. The UV-vis spectra shown in Figure 8A and C further confirm that a little amount of victoria blue B and methyl orange has been released into the water where aerogels were suspended. Interestingly, the rhodamine B composite aerogels is much more stable than the other ones because both from the photos or UV-vis spectrum (Figure 8B), no trace of the release of rhodamine B was observed. Moreover, after 3 month's exposure to light and air, there was still no trace of the release of rhodamine B (inset figure in Figure 8).

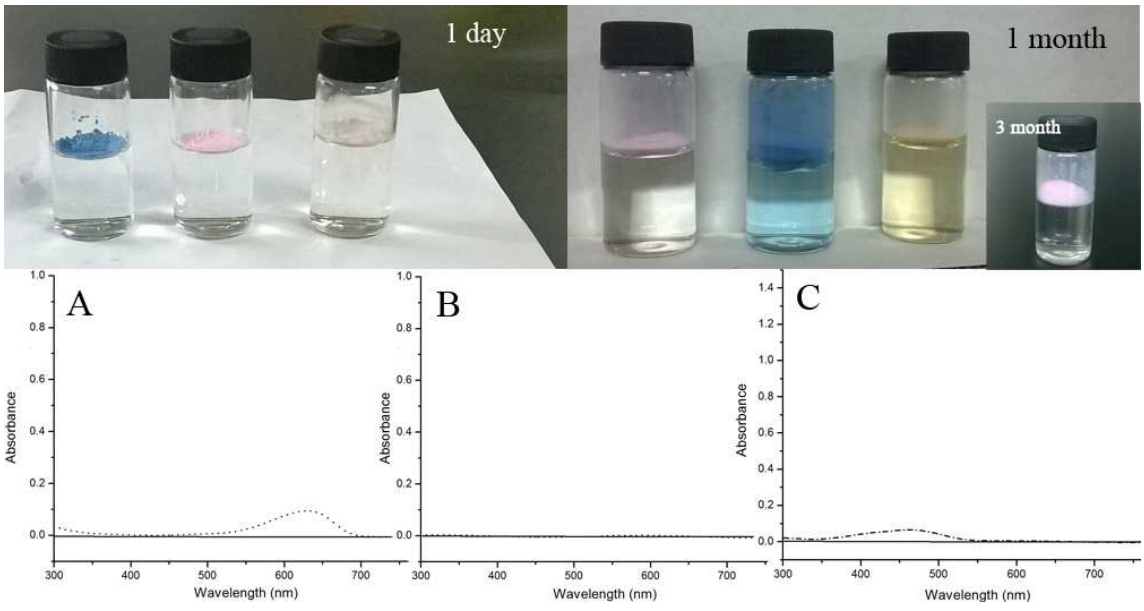

Figure 8. Photo images of aerogel powders in water at indicated times and the UV-vis spectra of the aqueous solution from: (A) Victoria blue B-silica composite aerogel sample (dotted line), (B) Rhodamine B-silica composite aerogel (dotted line), and (C) Methyl orange-silica composite aerogel (dotted line). The solid lines in the spectra are that of pure water.

3.3 Magnetic silica aerogels and their potential application to oil purification

Based on the successful synthesis of colored silica aerogels, we wonder if other functional silica aerogels would also be synthesized by this APD method. Therefore, the synthesis of magnetic silica aerogels, Fe_3O_4 nano-particles-silica composite aerogels, was investigated. However, two problems were soon recognized: (1) Fe_3O_4 is in soluble in ethanol and it's hard to be homogeneously dispersed in the wet-gel because the gels are usually formed by standing; and (2) when modified with TMCS, Fe_3O_4 particles were etched and Fe_3O_4-silica composite aerogels cannot be produced. In order to solve these problems, a relative larger amount of ammonium hydroxide was added in the sol-gel process to let the gelation occurred under vigorous stirring. After solvent-exchange with hexane, HMDS was used as the modification reagent. In these conditions, magnetic silica aerogels were successfully prepared by the APD method, the photo image of the aerogels is shown in Figure 9. The structure of the aerogels is confirmed by FTIR as shown in Figure 4g. Similar to the FTIR spectra of the silica aerogels and dye-silica composite aerogels, that of the Fe_3O_4-silica composite aerogels also exhibit two peaks at 840 and 1360 cm^{-1} that correspond to the vibrations of Si-C. Besides, the –OH peak at 3450 cm^{-1} is almost unobservable in the magnetic silica aerogels. The results clearly indicate that HMDS work efficiently for the APD of functional silica aerogels.

For a detailed investigation, the impacts of the contents of Fe_3O_4 and drying temperature on the structure and physical properties of the composite aerogels were studied. As presented in Table 3, two samples containing 2 wt% of Fe_3O_4 were dried at 80 and 150 ^oC, respectively. While another two samples containing 5 wt% of Fe_3O_4 were also dried at 80 and 150 ^oC, respectively. As can be seen in Table 3, the average pore diameter and pore volume increased

with higher drying temperature, while the density and thermal conductivity decreased, similar to that of pure silica aerogels. However, the BET surface areas are slightly decreased. Nevertheless, the values are comparable to that of silica aerogels and dye-composites aerogels, which indicate that the Fe_3O_4 nano-particles are successfully embedded in the silica networks. Moreover, the TEM image of composite aerogels (entry 10) shown in Figure 10 suggest that the Fe_3O_4 nano-particles are uniformly dispersed in the silica framework. As can be seen in Figure 10, the framework of the composite aerogels is made up by nano particle networks, and no obvious large aggregation domains have been observed.

Table 3. Structure and physical parameters of the Fe_3O_4-silica composite aerogels.

Entry[a]	Drying Temperature (^oC)	Density (mg/cm^3)	Surface areas (m^2/g)	Average pore diameter (nm)	Pore volume (cm^3/g)	Thermal conductivity (W/mK)
9[b]	80	95.2	695.27	10.3	2.02	0.0257
10[b]	150	78.1	679.76	14.6	2.72	0.0250
11[c]	80	106.0	563.40	13.7	2.22	0.0294
12[c]	150	83.0	542.19	18.27	2.79	0.0260

[a] The modification reagent is HMDS. [b] The feed weight ratio of Fe_3O_4 to silica is 2%. [c] The feed weight ratio of Fe_3O_4 to silica is 5%.

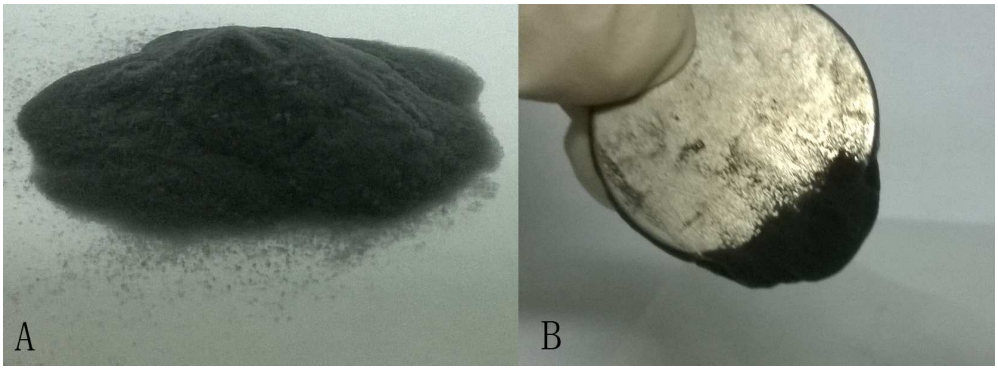

Figure 9. Photo images of magnetic aerogels, Fe_3O_4-silica composite aerogels (entry 10).

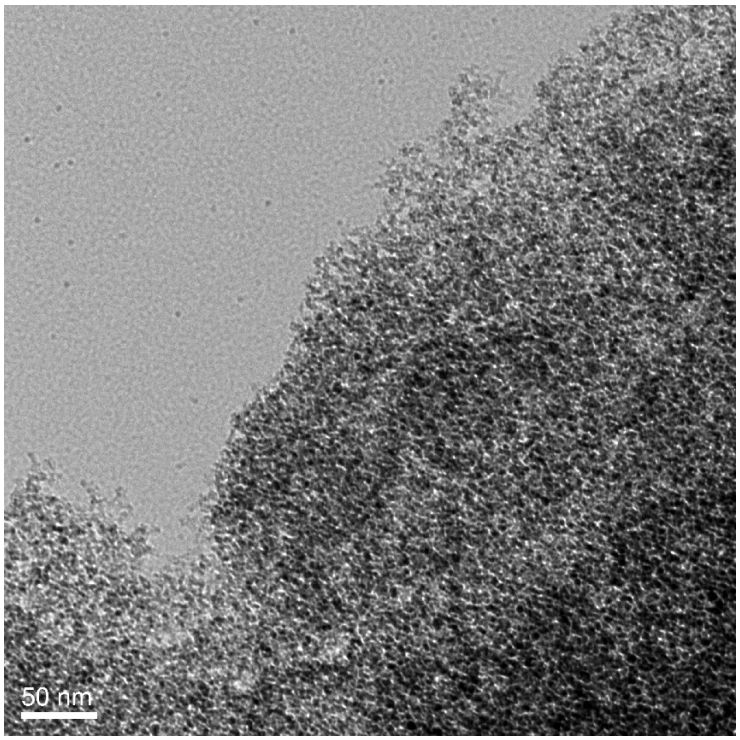

Figure 10. TEM image of Fe_3O_4-silica composite aerogels (entry 10)

The N_2 adsorption-desorption isotherms and pore size distribution of Fe_3O_4-silica composite aerogels are given in Figure 11. All the samples exhibit type IV isothems with hysteresis loops similar to that of pure silica aerogels, the results indicate that the shape of the pores of these composite aerogels are depend on the PEDS precursors while the embedded components are not critical for the pore shapes. This conclusion can be further confirmed by the isotherms traces of the dye-composite aerogels, as well as that of the Ag-composite aerogels that will be discussed in the next section.

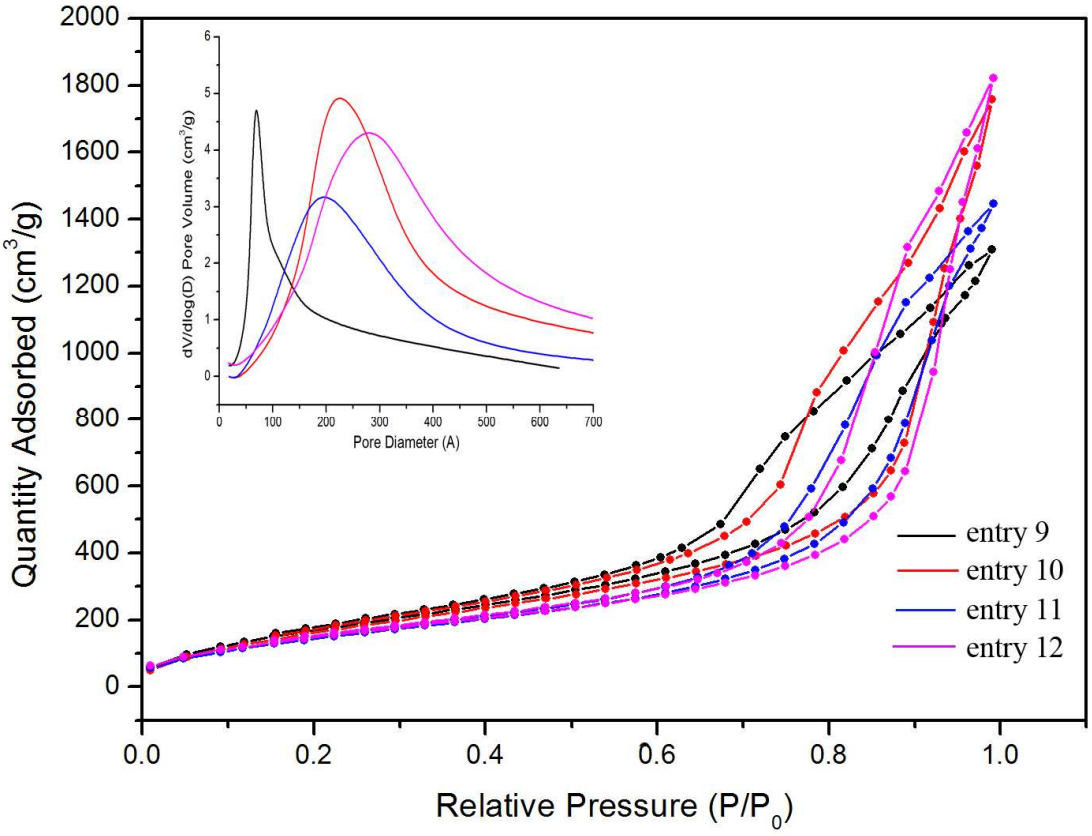

Figure 11. N_2 adsorption-desorption isotherms of Fe_3O_4-silica composite aerogels. The inserted figure is the pore size distributions of the corresponding aerogels.

Due to the interesting magnetic properties of the Fe_3O_4-silica composite aerogels, as well as their hydrophobicity and high pore volume, the wastewater treatment capacity of the aerogels were briefly investigated in this work. As a preliminary study, the adsorption of hexane by the composite aerogels was carried out. When 18.4 mg aerogels was used, up to 191.8 mg hexane can be adsorbed, which indicated that the adsorption capacity of the aerogels to hexane was more than 10 times by weight. Interestingly, as the aerogels are magnetic, they can be easily collected under a magnetic field after adsorption of hexane (Figure 12). Furthermore, while the aerogels were dispersed in large amount of hexane, it could be simply aggregated and collected by using a magnetic field.

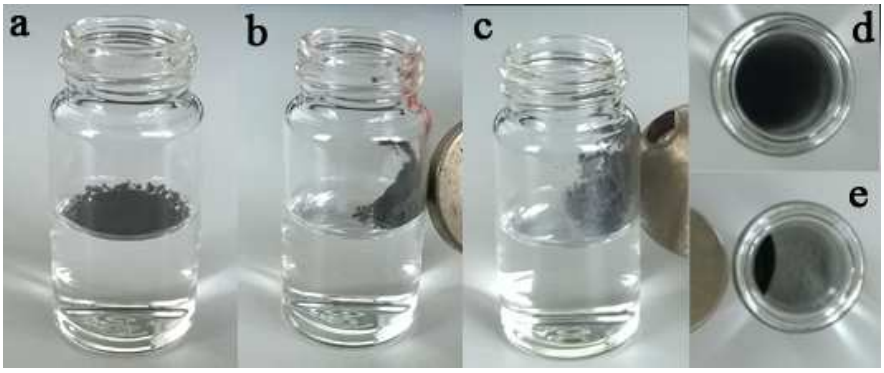

Figure 12. Photo images of the magnetic aerogels for hexane adsorption: (a) aerogel suspension in water; (b) aerogel adsorbed 2.5 times of hexane; (c) aerogel adsorbed 7 times of hexane; (d) aerogel dispersed in 105 times of hexane; and (e) aerogel aggregated in 105 time of hexane in a magnetic field

3.4 Ag nano-wire-silica composite aerogels and their physical properties

The versatility of the APD method has been approved by synthesizing various organic and inorganic composite silica aerogels, such as organic small molecules, metal ions, and nano-particles were all embedded in the silica networks by the APD method (only hexane-exchange and surface modification). In this section, we further demonstrated that nano-wires can also be embedded in the silica networks. Ag nano-wires were used in hope of that functional composite silica aerogels with electron-conductivity and sterilization etc. functions could be fulfilled. It's should be noted that the relative mild HMDS should be used as modification reagents, the TMCS can etch the Ag nano-wires due to the forming of HCl.

The impacts of the contents of Ag nano-wire and drying temperature on the structure and physical properties of the composite aerogels were investigated. As shown in Table 4, all the samples showing large BET surface areas higher than 640 m^2/g and high pore volume larger than 1.2 cm^3/g, regardless the introduction of Ag nano-wires. However, the tapping densities

(>100 g/cm^3) and thermal conductivities (mostly > 0.03 W/mK) of these aerogels are higher than that of silica aerogels and dye, Fe_3O_4 composite silica aerogels, this may be due to that facts that a higher content of Ag were used (8 %) and the PVP surfactants for the uniform distribution of Ag nano-wires were not washed out by hexane exchange. Nevertheless, the structure of the Ag-silica composite aerogels is not much affected.

Table 4. Structure and physical parameters of the Fe_3O_4-silica composite aerogels.

Entry[a]	Drying Temperature (^{o}C)	Density (mg/cm^3)	Surface areas (m^2/g)	Average pore diameter (nm)	Pore volume (cm^3/g)	Thermal conductivity (W/mK)
13[b]	80	148.2	722.49	8.76	1.83	0.0347
14[b]	150	105.3	734.38	12.89	2.67	0.0270
15[c]	80	194.0	667.0	6.64	1.23	0.0383
16[c]	150	162.7	642.62	9.16	1.69	0.0321

[a] The modification reagent is HMDS. [b] The feed weight ratio of Ag to silica is 5%. [c] The feed weight ratio of Ag to silica is 8 %.

The FTIR spectrum of Ag-silica aerogels (entry 14) shown in Figure 4f exhibits two peaks at 840 and 1360 cm^{-1} that correspond to the vibrations of Si-C, while the –OH peak at 3450 cm^{-1} is almost unobservable. This indicated that the –OH has been replaced by –Si(CH$_3$)$_3$ groups. The N_2 adsorption-desorption isotherms and pore size distribution of Ag-silica composite aerogels are presented in Figure 13. All the samples exhibit type IV isothems with hysteresis loops similar to that of the silica-based composite aerogels.

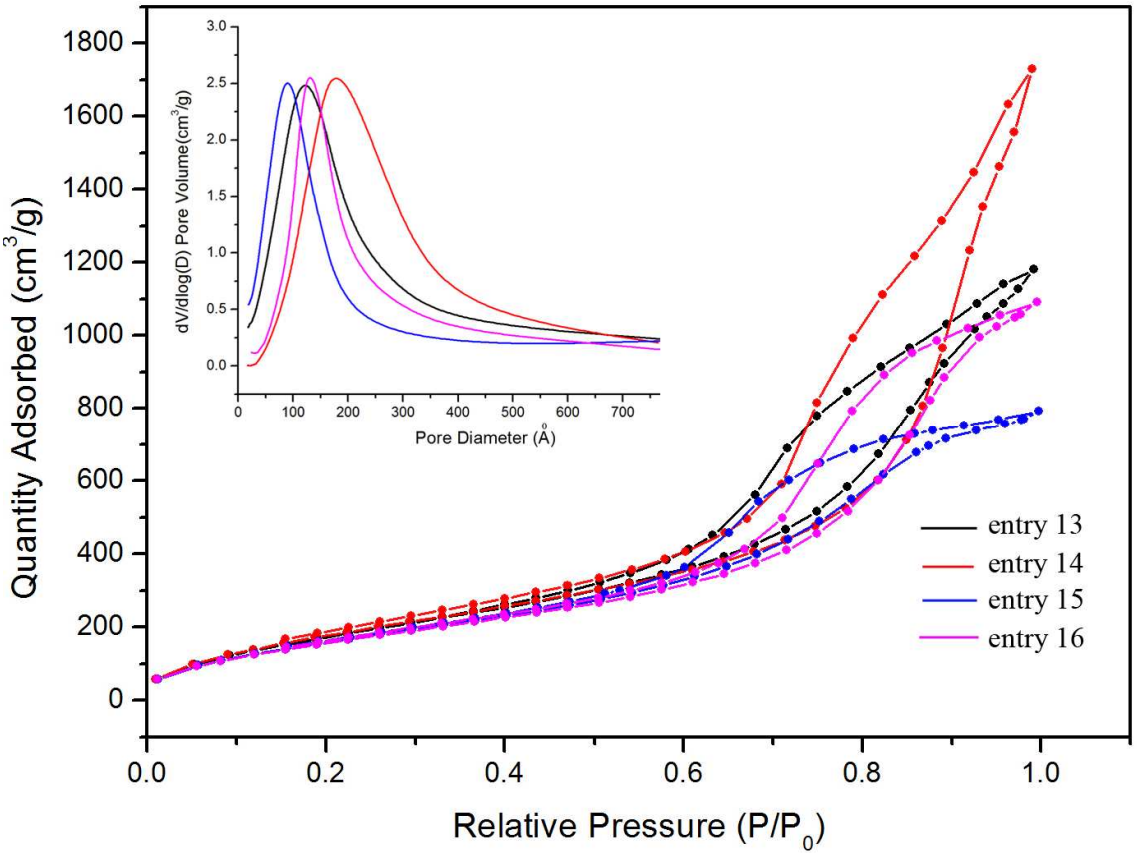

Figure 13. N_2 adsorption-desorption isotherms of Ag-silica composite aerogels. The inserted figure is the pore size distributions of the corresponding aerogels.

Though the Ag-silica composite aerogels are successfully synthesized, the electron-conducting measurement (not shown) indicates that the aerogels is electron insulation. We considered that the Ag content is low in the composite aerogels and no connecting networks of Ag nano-wires exist in the aerogels, therefore, the composite aerogels is electron insulating. To confirm this speculation, SEM measurement was performed. Figure 14 shows the images of the Ag composite aerogels (entry 14), the Ag nano-wires can be clearly identified (red circle) and are dispersed and embedded in the silica matrix. No Ag network is found and the composite aerogels is not electron-conduction.

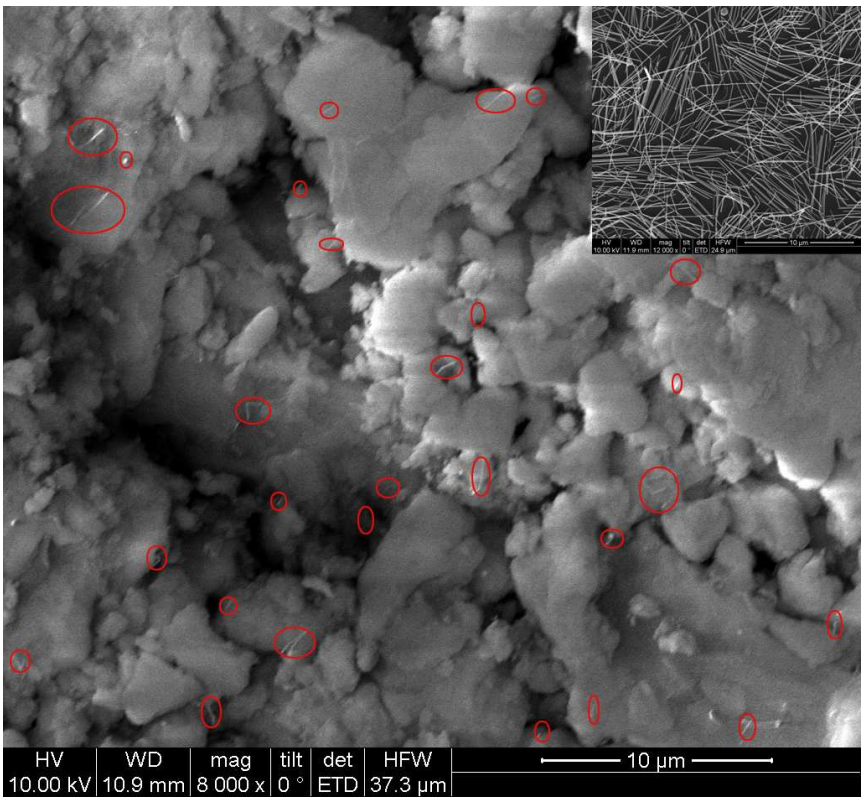

Figure 14. SEM image of Ag nano-wire-silica composite aerogel (insert is the SEM image of Ag nano-wire, Ag networks are formed by contacting and twining)

4. Conclusions

A versatile APD method of synthesized silica aerogels was developed in this work, where only hexane solvent-exchange was performed and a small amount of modification reagents were used. More over, the drying temperature is ranging from room temperature to 150°C, thus the ambient pressure and ambient temperature drying method is also reported. This APD method is cable of synthesizing various composites silica aerogels showing different colors and functions. All the silica and silica-based composite aerogels show high BET surface areas range from 500 to 1000 m^2/g and average pore sizes in the range of 8-20 nm, regardless of the drying temperature and the dye or nano-particles embedded. The tapping densities of the aerogels were in the range of 0.03 g/cm^3 to 0.2 g/cm^3, and the thermal conductivities were

found varying from 0.0221 to 0.04 W/mK. Besides, larger pore diameters can be achieved by increasing the drying temperature, while the pore shape of the composite areogels was found to depend on the precursors been used rather than the embedded components (such as organic dyes and metal nano-particles). The UV-vis measurement of colored silica aerogels indicates that the dyes are stable, and may be released rather slowly when continuous immersed in water for one month. The capacity of the magnetic aerogels for hexane adsorption is higher than 10 times by weight, and the aerogels can be easily collected under a magnetic field. In general, a versatile APD method was developed, due to the simplified process with only hexane-exchange, and the ability to synthesize various composite aerogels, this APD method is especially useful for industrial large-scale production of silica areogels.

Acknowledgments

This work was financially supported by the National Natural Science Foundation of China (21373024), the Innovation Program of the Beijing Institute of Technology and the 100 Talents Program of the Chinese Academy of Sciences.

References

1 J. Fu, Y. Zhu, Y. Zhao, *J. Mater. Chem. B*, 2014, **2**, 3538-3548.

2 R. Ravichandran, D. Sundaramurthi, S. Gandhi, S. Sethuraman, U. M. Krishnan, *Microporous Mecroporous Mater.*, 2014, **187**, 53-62.

3 Y. Yamauchi, T. Kimura, *Chem. Comm.*, 2013, **49**, 11424-11426.

4 M. Wang, X. Wang, Q. Yue, Y. Zhang, C. Wang, J. Chen, H. Cai, H. Lu, A. A. Elzatahry, D.

Zhao, Y. Deng, *Chem. Mater.,* 2014, 26, 3316-3321.

5 N. Linares, A. M. Silvestre-Albero, E. Serrano, J. Silvestre-Albero, J. Garcia-Martinez, *Chem. Soc. Rev.,* 2014, DOI: 10.1039/c3cs60435g.

6 T. J. Ha, H. H. Park, H. W. Jang, S. J. Yoon, S. Shin, H. H. Cho, *Microporous Mecroporous Mater.,* 2012, **158**, 123-128.

7 P. B. Sarawade, J. K. Kim, A. Hilonga, H. T. Kim, *Solid State Sci.,* 2010, **12**, 911-918.

8 A. V. Rao, N. D. Hegde, H. Hirashima, *J. Colloid Interface Sci.*, 2007, **305**, 124-132.

9 S. S. Kistler, *Nature,* 1931, **127**, 741-741.

10 S. S. Kistler, *J. Phys. Chem.,* 1932, **36**, 52-64.

11 D.M. Smith, A. Maskara, U. Boes, *J. Non-Cryst. Solids*, 1998, **225**, 254-259.

12 L. Kocon, F. Despetis, J. Phalippou, *J. Non-Cryst. Solids,* 1998, **225**, 96-100.

13 A. Soleimani Dorcheh, M. H. Abbasi, *J. Mater. Processing Techn.,* 2008, **199**, 10-26.

14 M. A. Aegerter, N. Leventis, M. M. Koebel (Eds), *Aerogels Handbook*, Springer, 2011.

15 R. Baetens, B. P. Jelle, A. Gustavsen, *Energy Build.,* 2011, **43**, 761-769.

16 D. Sanli, C. Erkey, *ACS Appl. Mater. Interfaces,* 2013, **5**, 11708-11717.

17 J. C. H. Wong, H. Kaymak, S. Brunner, M. M. Koebel, *Microporous Mesoporous Mater.,* 2014, **183**, 23-29.

18 S. S. Prakash, C. J. Brinker, A. J. Hurd, S. M. Rao, *Nature*, 1995, **374**, 439-443.

19 S. D. Bhagat, Y. H. Kim, Y. S. Ahn, J. G. Yeo, *Microporous Mecroporous Mater.,* 2006, **96**, 237-244.

20 A. V. Rao. A. P. Rao, M. M. Kulkarni, *J. Non-Cryst. Solids*, 2004, **350**, 224-229.

21 P. B. Sarawade, J. K. Kim, A. Hilonga, H. T. Kim, *Powder Tech.,* 2010, **197**, 288-294.

22 S. D. Bhagat, K. T. Park, Y. H. Kim, J. S. Kim, J. H. Han, *Solid State Sci.,* 2008, **10**, 1113-1116.

23 K. Kanamori, M. Aizawa, K. Nakanishi, T. Hanada, *Adv. Mater.,* 2007, **19**, 1589-1593.

24 H. B. Chen, Y. Z. Wang, D. A. Schiraldi, *ACS Appl. Mater. Interfaces,* 2014, **6**, 6790-6796.

25 J. Kuhn, T. Gleissner, M. C. Arduini-Schuster, S. Korder, J. Frincke, *J. Non-Cryst. Solids,* 1995, **186**, 291-295.

26 M. Liu, L. Gan, Y. Pang, Z. Xu, Z. Hao, L. Chen, *Colloids Surfaces A*, 2008, **317**, 490-495.

27 L. Kocon, F. Despetis, J. Phalippou, *J. Non-Cryst. Solids,* 1998, **225**, 96-100.

28 T. M. Tillotson, L. W. Hrubesh, *J. Non-Cryst. Solids*, 1992, **145**, 44-50.

29 J. C. H. Wong, H. Kaymak, S. Brunner, M. M. Koebel, *Microporous Mesoporous Mater.,* 2014, **183**, 23-29.

30 D. Sanli, C. Erkey, *ACS Appl. Mater. Interfaces,* 2013, **5**, 11708-11717.

31 G. M. Pajonk, E. Elaloui, P. Achard, B. Chevalier, J. L. Chevalier, M. Durant, *J. Non-Cryst. Solids,* 1995, **186**, 1-8.

32 Y. G. Sun, B. Gates, R. Mayers, Y. N. Xia, *Nano Lett.,* 2002, **2**, 165-268.